J Digit Imaging (2015) 28:338–345
DOI 10.1007/s10278-014-9736-6

Evaluation of Back Projection Methods for Breast Tomosynthesis Image Reconstruction

Weihua Zhou · Jianping Lu · Otto Zhou · Ying Chen

Published online: 11 November 2014

Abstract Breast cancer is the most common cancer among women in the USA. Compared to mammography, digital breast tomosynthesis is a new imaging technique that may improve the diagnostic accuracy by removing the ambiguities of overlapped tissues and providing 3D information of the breast. Tomosynthesis reconstruction algorithms generate 3D reconstructed slices from a few limited angle projection images. Among different reconstruction algorithms, back projection (BP) is considered an important foundation of quite a few reconstruction techniques with deblurring algorithms such as filtered back projection. In this paper, two BP variants, including α-trimmed BP and principal component analysis-based BP, were proposed to improve the image quality against that of traditional BP. Computer simulations and phantom studies demonstrated that the α-trimmed BP may improve signal response performance and suppress noise in breast tomosynthesis image reconstruction.

Keywords Mammography · Digital breast tomosynthesis (DBT) · Back projection (BP) · α-Trimmed method · Principal components analysis (PCA)

W. Zhou · Y. Chen (✉)
Department of Electrical and Computer Engineering, Southern Illinois University Carbondale, 1230 Lincoln Drive, MC 6603, Carbondale, IL 62901, USA
e-mail: adachen@siu.edu

J. Lu · O. Zhou
Department of Physics and Astronomy, Curriculum in Applied Sciences and Engineering, The University of North Carolina, Chapel Hill, USA

J. Lu · O. Zhou
Lineberger Comprehensive Cancer Center, The University of North Carolina, Chapel Hill, USA

Introduction

Breast cancer accounts for around 30 % of all female cancers in the USA [1]. Early detection of breast cancer is viewed as the best hope to decrease breast cancer mortality [2]. It is universally accepted that mammography is the most efficacious tool for the early detection of breast cancer. With traditional mammography technique, the object is projected onto the detector or film to generate the 2D projection image of the breast. Superimposed objects on the projection images, caused by overlapped anatomical structures, bring limitations to mammography [3, 4], such as 20 % false-negative rates and high recall rates, which may result in unnecessary anxiety to the patients and increase the medical costs.

Compared to the standard mammography, digital breast tomosynthesis (DBT) technique may overcome the limitations by removing the ambiguities of overlapped tissues and providing the 3D localization. Since 3D slice images of the breast can be partially reconstructed based on a few limited angle projection images, DBT has the potentials to help decrease recall rates, improve the accuracy of breast cancer detection, and therefore reduce the number of women who die from such cancer [4].

In the process of tomosynthesis technique, sequences of limited angle 2D projection images are acquired first and then reconstructed into slice images of the breast. A few image reconstruction algorithms have been investigated by various research groups, including back projection (BP) reconstruction algorithm [5], filtered back projection (FBP) algorithm [6], matrix inversion tomosynthesis (MITS) [7], maximum likelihood expectation maximization (MLEM) [8, 9], simultaneous algebraic reconstruction techniques (SART) [10, 11], etc. Compared to other reconstruction algorithms, FBP runs very fast, enhances the conspicuity of objects, and removes out-of-plane artifacts [6, 11–15], therefore, it is extensively used in the current digital breast tomosynthesis systems. BP is a critical component of FBP and significantly influences the

image quality of FBP-reconstructed images [5, 6, 12, 16]. This paper focuses on investigation of BP algorithms.

Two BP variants, including α-trimmed BP and principal component analysis-based (PCA) BP, were proposed. Their performance of improving the conspicuity of lesions and suppressing noise was studied by computer simulations and phantom experiments.

Methods and Materials

Tomosynthesis Reconstruction Methods

The shift-and-add (SAA) tomosynthesis reconstruction algorithm [5] is a common mathematical method. It reconstructs the plane at the specified height by lining up each projection image according to its relative shift amount. When the X-ray beam is turned on, objects at different locations above the detector will be projected onto the detector at positions depending on the relative locations of the objects.

In order to reconstruct 3D slices of the breast, each projection image should be shifted by an amount appropriate for the plane of reconstruction. When the detector remains stationary and the tubes are in a plane that is parallel to the detector plane, the magnification of objects depends on the height of the object. With SAA reconstruction, shift amount for each projection image is calculated along the direction of X-ray tube movement. The shift amount can be calculated based on projected positions from central points of each reconstruction plane. The shifted planes are added together to emphasize structures in the in-focus plane and blur out structures in other planes.

Figure 1 shows a parallel tomosynthesis imaging geometry. The SAA uses Shift(O) as the shift amounts of all the pixels on the reconstruction plane S. For a specific projection image acquired by the X-ray source R, in order to shift the projection image to line up structures in the plane S, the SAA algorithm uses the shift amount calculated as

$$\text{shift}_i(S) = \text{shift}(O) = \frac{H}{\text{SID}-H}\cdot(R_x - O_x) \tag{1}$$

One can obtain the reconstructed plane S as the average of all the shifted projection images [5, 14].

Traditional BP Method

The 3D reconstructed slices can be acquired from the SAA algorithm. Nevertheless, because the different pixels on the reconstruction plane have their unique locations, the shift amounts should be different. In order to improve the reconstruction of the single pixel on a reconstruction plane at certain height above the detector, the shift amount should be calculated along both x and y directions for each pixel on the reconstruction plane. This is called the point-by-point back projection [5].

With the point-by-point back projection, shift amounts for every pixel location on each reconstructed plane are computed, taking into account the 2D projection of reconstructed objects in each plane. Figure 2 illustrated such a procedure. The location equation between the reconstructed point A and its projection point B is written as

$$\begin{aligned} B_x &= R_x + \frac{R_z}{R_z - A_z}\cdot(A_x - R_x) \\ B_y &= R_y + \frac{R_z}{R_z - A_z}\cdot(A_y - R_y) \end{aligned} \tag{2}$$

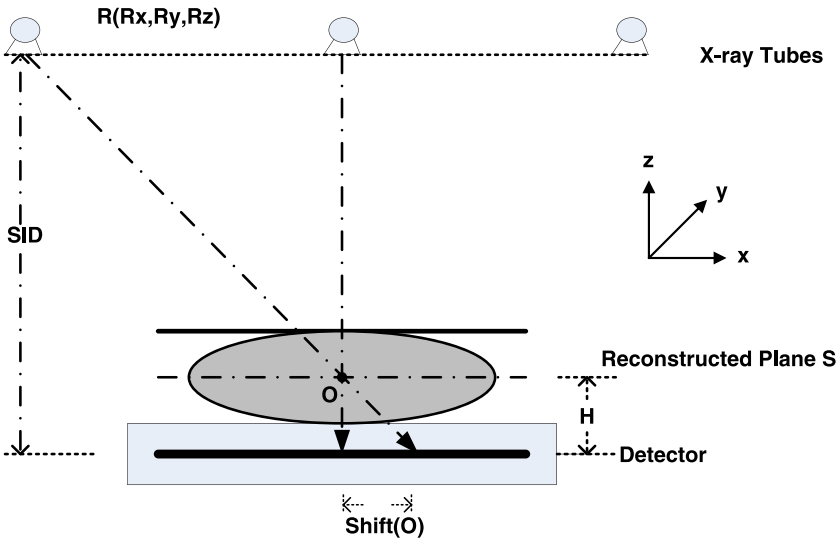

Fig. 1 Imaging geometry of a parallel X-ray breast tomosynthesis system. The X-ray tubes were placed along the top horizontal line. SID is the distance from X-ray tubes to the detector plane. The plane S represents a reconstruction plane at a height of H above the detector surface. When the X-ray beam is turned on, objects in the plane S will be projected onto the detector. *R*, the location of X-ray tube; *O*, the center of the reconstructed plane S; *Shift(O)*, the shift amount of the point O when the X-ray projection line RO passes through the plane S

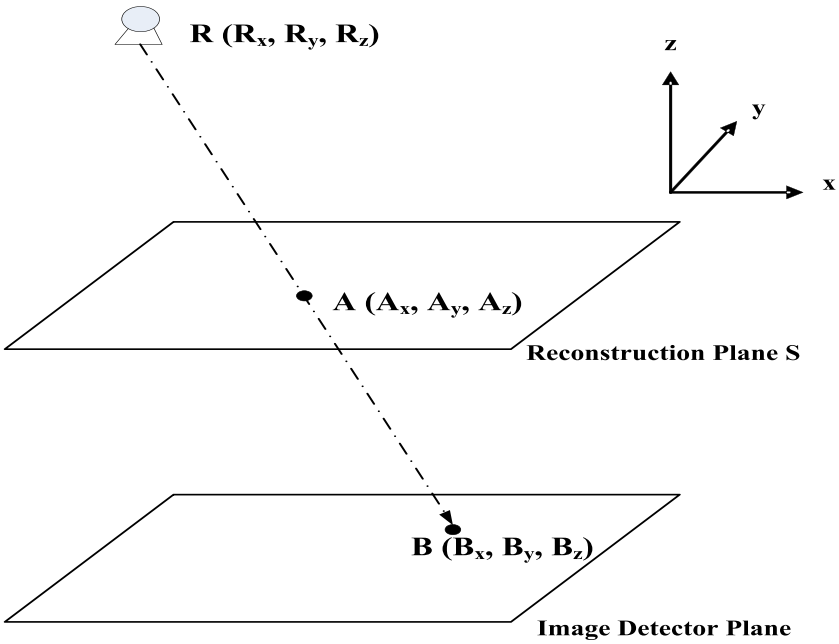

Fig. 2 Projection geometry. *R*, the location of X-ray source; *A*, a point on the reconstruction plane S; *B*, projection location of *A* on the detector plane

The back-projected pixels represent the estimation about the internal structure of the object. For each projection image, we can acquire a corresponding estimation. The actual structure can be approximated from all the estimations. The final pixel value of the point A in the traditional BP algorithm is the mean value of the back-projected pixels from all the N projection images (N is the number of projection images).

Traditional BP is capable of improving the conspicuity of in-plane object and decreasing out-of-plane artifacts against SAA [5]. In order to utilize the statistical properties of those N values and thus improve the image quality, two variants were proposed as below.

α-Trimmed Method

The α-trimmed BP removes the "extremity" values in the back-projected pixels. In the implementation, we sorted all the pixel values in the back projection images, removed the d/2 lowest and the d/2 highest gray-level values, and then calculated the mean value. It can be written as

$$s = \frac{1}{N-d} \sum_{i=d/2+1}^{N-d/2} I(B_i) \tag{3}$$

where the value of d can range from 0 to N−1. When d=0, the α-trimmed method regresses to traditional BP. If we choose d=N−1, it becomes a median BP. This technique is often used to remove mixed noise in digital image processing [16].

PCA-Based Method

The PCA method is an eigenvector-based multivariate analysis technique, and it provides an orthogonal linear transformation from n-dimensional coordinate system to a new m-dimensional coordinate system ($m<n$). It is performed in such a way that a truncation of an input vector in the new coordinate system only causes a minimal square error, i.e., a minimal loss of information [17]. PCA has been served as a standard tool for a large diversity of data analysis and information visualization to extract the most important information [16, 17]. In our PCA-based BP implementation, the first principal eigenvectors of the matrix being composed of the N back-projected pixel values were calculated as the reconstructed image.

Digital Breast Tomosynthesis Prototype System

A new multi-beam breast tomosynthesis prototype system, invented by Zhou et al. [18], was used for our phantom experiments. The system used static multi-beam X-ray emitters as the sources and controlled the X-ray sources by electronic switches.

In the investigated prototype system, 15 X-ray sources, operated at a voltage of 30 kV, were linearly fixed along a parallel line above the detector, as illustrated in Fig. 1. In this paper, the detector had a pixel pitch of 140 μm. The image size was 2048×1664. The distance from the X-ray tubes to the

detector (SID) was around 690 mm. The total view angle θ is equal to 15°. In all the following experiments, d was set to be 4 in order to reduce noise as well as to keep the detected pixel intensity.

Experiments

Breast Phantom

A standard breast biopsy training phantom [19] was used in this experiment. The phantom was composed of a proprietary gel similar to human tissue. Dense masses and micro-calcifications with varied sizes were embedded into the phantom. To evaluate the tomosynthesis imaging of the biopsy training breast phantom, 15 low dosage projection images at a total exposure of 80 mAs (5.3 mAs/projection) were obtained and reconstructed by the investigated algorithms.

Masses and micro-calcifications were extracted from the reconstructed images. The contrast-to-noise ratio (CNR) [11] was used to quantitatively compare the reconstruction algorithms based on the reconstructed regions of interest (ROI). It was defined by

$$\mathrm{CNR} = \frac{\mu_{\mathrm{ob}} - \mu_{\mathrm{bg}}}{\sigma_{\mathrm{bg}}} \tag{4}$$

where μ_{ob} and μ_{bg} are the mean pixel values of the object and image background, respectively, and σ_{bg} is the root mean square noise value of pixel values in the image background.

Spherical Object Simulation

A spherical object with the radius of 0.4 mm, placed at the height of 20 mm above the detector, was simulated and embedded in a uniform background as the target-to-test reconstruction algorithms. The linear attenuation coefficient of the simulated spherical object was set as 0.038/mm, which referred to the linear attenuation coefficient of carcinoma tissue for 30 KeV photon energy [20]. Ray tracing method was used to model the X-ray attenuation.

Three groups of simulation were conducted to test the response of the algorithms:

1. In the first simulation, a solid sphere was put in the center above the detector plane, the background was uniform, and we did not add any noise to the simulated data.
2. In the second simulation, mixed noise (Gaussian and salt-and-pepper noise) was added to every projection image of the first group to reveal the performance of noise removal with the investigated reconstruction algorithms.
3. In the third simulation, a solid sphere was placed near the boundary of the reconstruction plane. Due to limited size of the detector, part of the sphere was projected out of the detector. This simulation was expected to demonstrate if the algorithms could preserve the shape of the object when it was near the boundary and some portions of the object could go beyond the detector when projected.

The above three BP algorithms were then applied to reconstruct the images acquired from simulated tomosynthesis datasets. A reconstruction plane spacing of 1 mm was used. An in-plane line passing through the center of the sphere along the horizontal axis and the out-of-plane line parallel to and 4 mm above the in-plane were extracted to evaluate the out-of-plane removal of the investigated reconstruction algorithms.

Noise Power Spectrum (NPS) Measurement

To measure the noise propagation in the reconstructed images as a function of spatial frequency, noise power spectrum (NPS)(f) was tested with the DBT prototype system. A standard phantom (47 % water and 53 % adipose equivalent) with the equivalent distribution of attenuation and scatter radiation in breast tissues was placed on the surface of the detector. The projection images were acquired by our prototype system with the same exposure and imaging configuration as in the biopsy phantom experiment and reconstructed by the three investigated reconstruction algorithms.

The NPS(f) investigation with the reconstruction algorithms used a 1D NPS line profile method [11]. It cuts the ROIs with 1024×1024 pixels from the reconstructed planes with the same height above the detector. Each ROI was evenly divided into 63 strips with a size of 1024×32 pixels. The adjacent strips were overlapped. For each strip, a line curve fitting was used to obtain an approximation to the true NPS. Finally, we extracted the frequency components from each strip and formed the smoothened NPS curves.

In our implementation, the reconstructed plane containing the ROI for NPS(f) estimation was 45 mm above the detector. The measurement of the 1D NPS was repeated on two experiments of the phantom at the same plane and the average of the repeated measurement was compared.

MTF Measurement

To characterize signal propagation in the investigated reconstruction algorithms, MTF(f) was tested. We used an impulse response simulation method [21]. In our measurement, an impulse, located at the center of the plane which is 45.0 mm above the detector, was computer simulated with the imaging configuration of the prototype system. The intensities of the X-ray projection lines which passed through the simulated

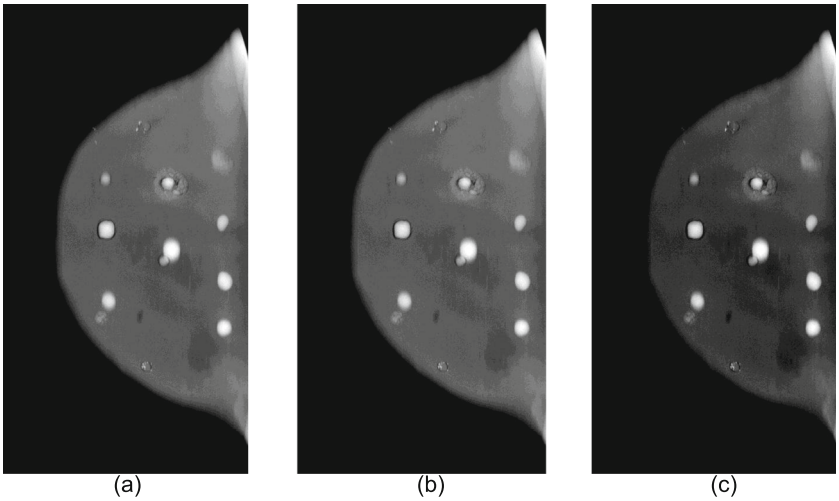

Fig. 3 Reconstructed slice images of the biopsy phantom. **a** Traditional BP, **b** α-trimmed BP, **c** PCA-based BP

impulse point were reduced by an amount of 1000 when forming the projection images. Impulses were then reconstructed by the above three algorithms. In MTF(f) calculation, the reconstructed slices 45.0 mm above the detector were selected. FFT transform of the slices was calculated to extract frequency components and generate the MTF curves.

Results

Phantom Study

Figure 3 shows the reconstructed plane that is 47.0 mm above the detector. Figure 4 shows reconstructed ROIs from traditional BP, α-trimmed BP, PCA-based BP respectively.

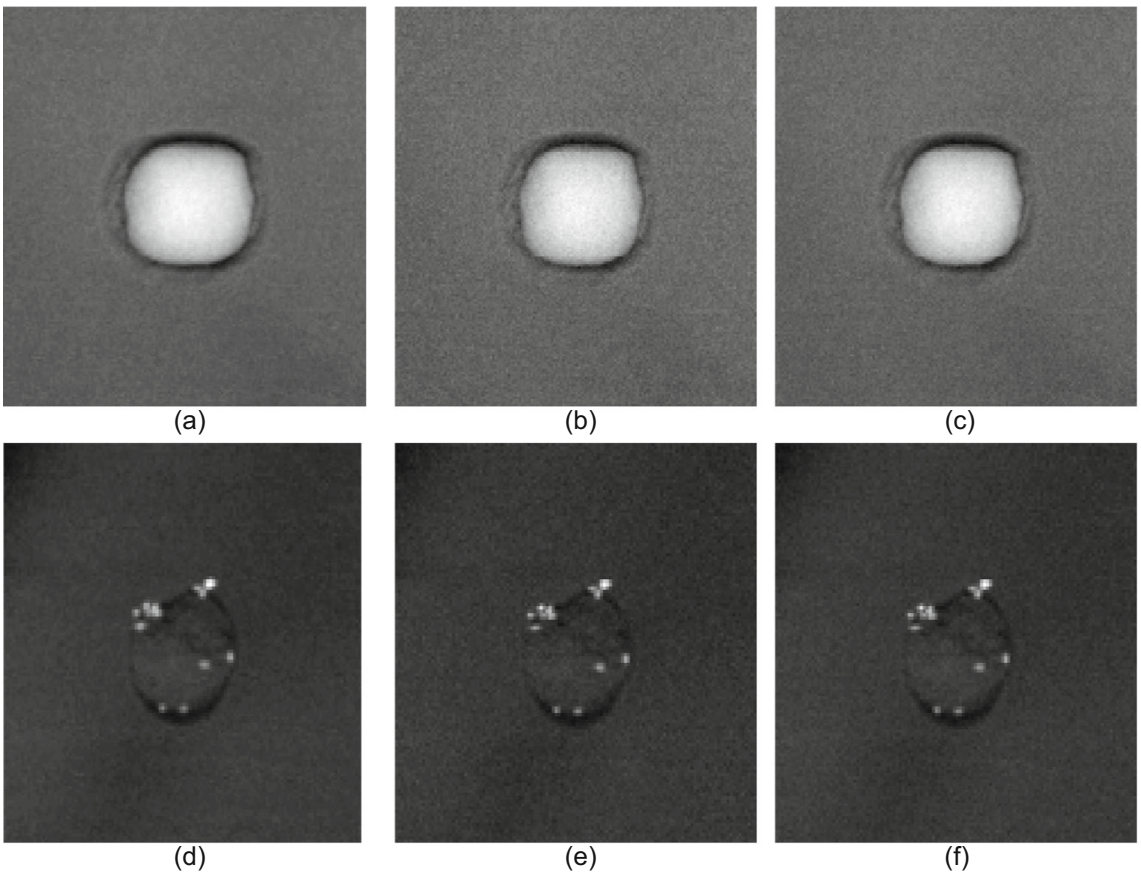

Fig. 4 Reconstructed regions of interest in the phantom. **a**, **b**, **c** Masses reconstructed by traditional BP, α-trimmed BP, and PCA-based BP, respectively. **d**, **e**, **f** Microcalcifications reconstructed by traditional BP, α-trimmed BP and PCA-based BP, respectively

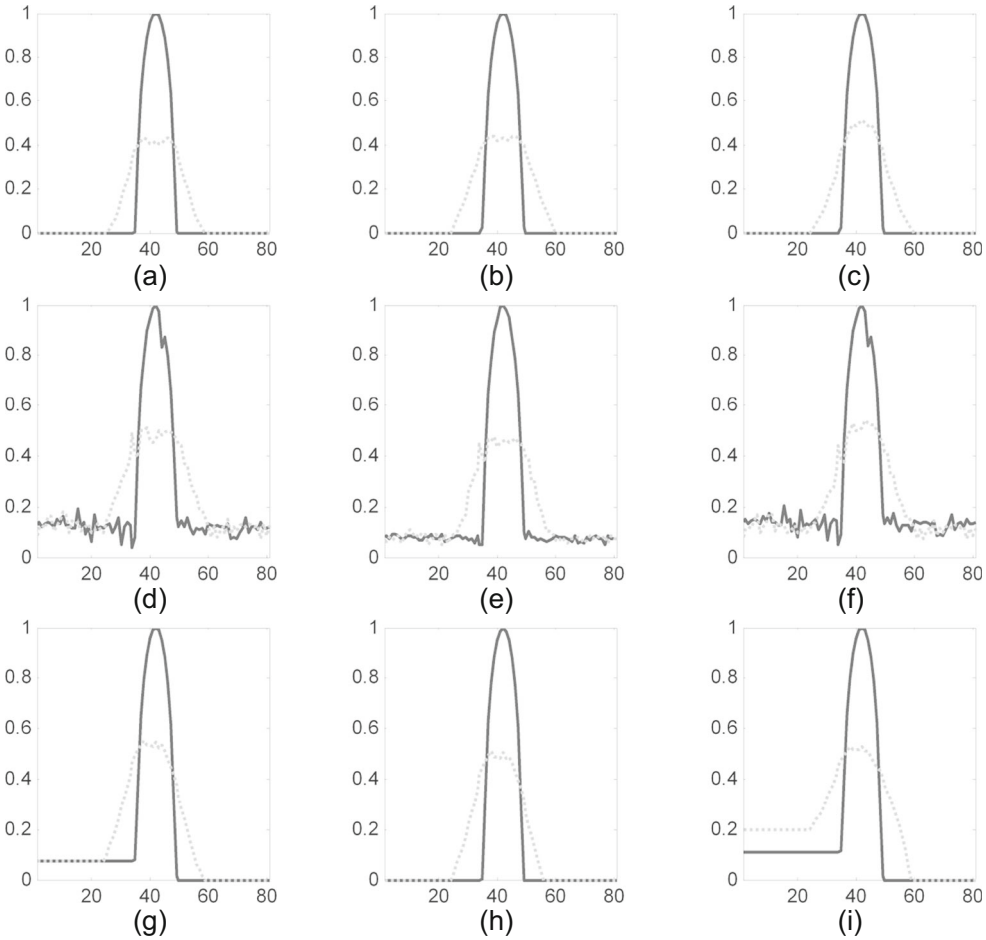

Fig. 5 In-plane and out-of-plane line profiles of reconstructed spheres in the three groups of simulation. **a**, **b**, **c** Simulation without noise; **d**, **e**, **f** simulation with the mixed noise; **g**, **h**, **i** Simulation with a near-boundary sphere. **a**, **d**, **g** Reconstructed by traditional BP; **b**, **e**, **h** Reconstructed by α-trimmed BP; **c**, **f**, **i** Reconstructed by PCA-based BP. *Solid lines* are the ones that pass through the center of the simulated spherical object and are in-plane line profiles. *Dotted lines* are the ones that are parallel to the in-plane lines but 3 mm higher, and they are out-of-plane line profiles. *X*-axis represents the pixel location. *Y*-axis represents the pixel intensity. For each reconstruction algorithm, the pixel intensities were normalized based on the in-plane (H=20 mm) maximum pixel intensity

All the three reconstruction algorithms were capable of providing 3D reconstruction of the phantom with the location, shape, and edge information. The breast phantom was compressed to be around 4 cm, therefore, in the micro-calcification cluster, not all the micro-calcification points were at the same planes, so some got blurred. This revealed the 3D localization of tomosynthesis reconstruction.

CNR values of the masses from Fig. 4 were 2.68, 2.81, and 2.76 for traditional BP, α-trimmed BP, PCA-based BP, respectively. The α-trimmed BP shows higher conspicuity for reconstructed objects.

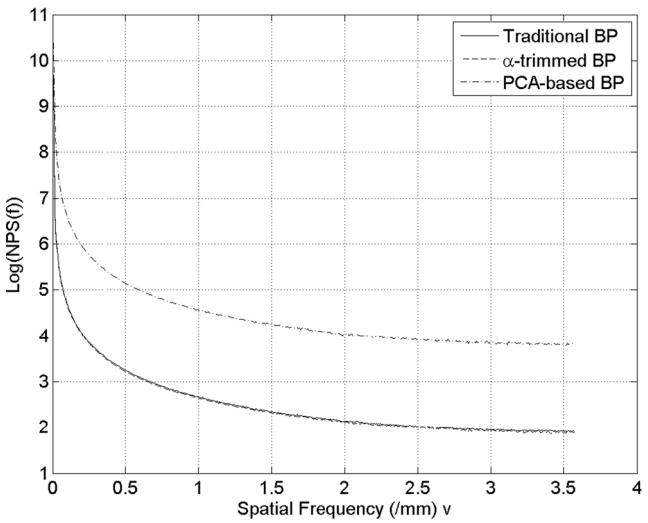

Fig. 6 NPS(f) curves of different reconstruction algorithms

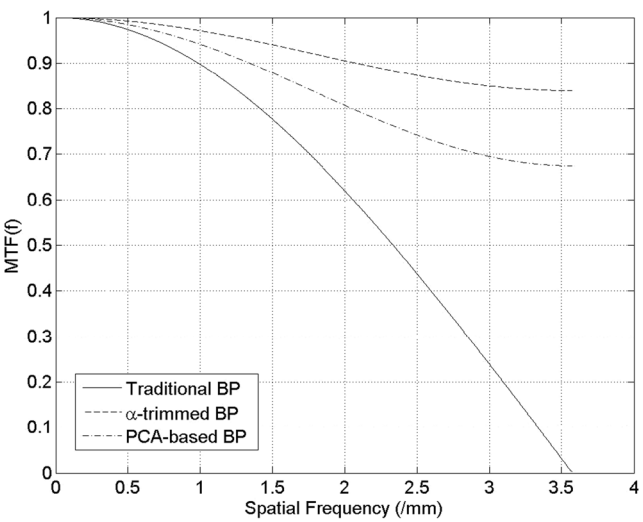

Fig. 7 MTF(f) curves of different reconstruction algorithms

Spherical Object Simulation

For each reconstruction algorithm (traditional BP, α-trimmed BP, and PCA-based BP) and computer simulation, two line profiles of normalized pixel intensities on the defined reconstruction planes were shown in Fig. 5.

In the simulation without noise (Fig. 5a–c), results from α-trimmed and traditional BP were quite similar. The result of PCA-based BP had higher out-of-plane blur. Artifact spread function (ASF) was used to evaluate the removal of out-of-plane blur. It was the difference between the in-plane average pixel values and out-of-plane average pixel values. ASF values were 0.41, 0.43, and 0.36 for traditional BP, α-trimmed BP, PCA-based BP, respectively.

In the simulation with mixed noise (Fig. 5d–f), the line profiles of α-trimmed BP were much smoother than the ones of traditional BP and PCA-based BP. CNR was measured for 1D in-plane line profiles and it was 0.82, 0.97, and 0.88 for traditional BP, α-trimmed BP, and PCA-based BP, respectively.

In the simulation with near-boundary sphere (Fig. 5g–i), α-trimmed BP preserved the shape of near-boundary object, while traditional BP and PCA-based BP could not reveal ambiguities when viewing the objects near the boundary of the reconstruction plane.

NPS Measurement

The average 1D NPS in the same selected area is shown in Fig. 6 for the three reconstruction methods. Fifty percent of maximum NPS(f) was 0.11, 0.11, and 0.54 for traditional BP, α-trimmed BP, PCA-based BP, respectively. The traditional BP and α-trimmed BP methods produced the essentially indistinguishable NPS(f) level in the reconstructed slice. PCA-based BP had higher spatial frequency response since it intends to maximize the information retrieval.

MTF Measurement

The α-trimmed BP had the maximal MTF(f) for all the frequencies, as shown in Fig. 7. The 10 % MTF(f) drop-off was 0.99 for traditional BP, 2.08 for α-trimmed BP, and 1.34 for PCA-based BP.

Conclusions

Masses and micro-calcifications were revealed in the 3D reconstructed images by the investigated reconstruction algorithms, including traditional BP, α-trimmed BP, and PCA-based BP. Among the investigated algorithms, the α-trimmed BP has better capability to reduce noise and out-of-plane artifact and thus improve the conspicuity of in-plane objects. In addition, the α-trimmed BP contributes to preserve the shape of the near-boundary object. Nevertheless, the value of α should be carefully selected to maximize the performance of the α-trimmed BP algorithm. A fixed value of α was used for our experiments, but it may have to be tuned when being applied in the other tomosynthesis imaging system.

FBP with the α-trimmed BP as the back projection step has the potential to improve the image quality of reconstructed slices. Next step, we will implement it in our FBP reconstruction algorithm. Phantom studies and clinical data will be used to validate our new algorithm.

References

1. Highnam R, Brady M (1999) Mammographic Image Analysis. Kluwer Academic Publishers, Dordrecht, The Netherlands
2. Nass SJ, Henderson IC, Lashof JC (2001) Mammography and Beyond: Developing Technologies for the early Detection of Breast Cancer. National Academy Press, Washington, DC
3. Niklason LT, Christian BT, Niklason LE, Kopans DB, Castleberry DE, Opsahl-Ong BH, Landberg CE, Slanetz PJ, Giardino AA, Moore RH, Albagi D, DeJule MC, Fitzgerald PA, Fobare DF, Giambattista BW, Kwasnick RF, Liu J, Lubowski SJ, Possin GE, Richotte JF, Wei CY, Wirth RF (1997) Digital tomosynthesis in breast imaging. Radiology 205:399–406
4. Park JM, Franken EA, Garg M, Fajardo LL, Niklason LT (2007) Breast tomosynthesis: present considerations and future applications. Radiographics 27(Suppl 1):231–240
5. Chen Y, Lo JY, Dobbins JT III (2007) Importance of point-by-point back projection (BP) correction for isocentric motion in digital breast tomosynthesis: Relevance to morphology of microcalcifications. Med Phys 34(10):3885–3892
6. Mertelemeier T, Orman J, Haerer W, Dudam MK (2006) Optimizing filtered backprojection reconstruction for a breast tomosynthesis prototype device. Proc SPIE 6142:131–142
7. Chen Y, Lo JY, Dobbins JT III (2004) Matrix Inversion Tomosynthesis (MITS) of the Breast: Preliminary Results. RSNA 90th Scientific Assembly, Chicago, IL
8. Wu T, Stewart A, Stanton M, McCauley T, Philips W, Kopans DB, Moore RH, Eberhard JW, Opsahl-Ong B, Niklason L, Williams MB (2003) Tomographic mammography using a limited number of low-dose cone-beam projection images. Med Phys 30:365–380
9. Zhou W, Balla A, Chen Y (2008) Tomosynthesis Reconstruction Using an Accelerated Expectation Maximization Algorithm with Novel Data Structure Based on Sparse Matrix Ray-Tracing Method. Int J Funct Inform Personalised Med 1(4):355–365
10. Andersen AH (1989) Algebraic reconstruction in CT from limited views. IEEE Trans On Med Imaging 8(1):50–55
11. Zhang Y, Chan H, Sahiner B, Wei J, Goodsitt MM, Hadjiiski LM, Ge J, Zhou C (2006) A comparative study of limited-angle cone-beam reconstruction methods for breast tomosynthesis. Med Phys 33(10): 3781–3795
12. Chen Y, Zhou W, Yang G, Lu JP, Zhou O (2009) Breast tomosynthesis reconstruction with a multi-beam x-ray source. Proc SPIE 7258:725859–7258568
13. Zhou W, Xin Q, Lu JP, Zhou O, Chen Y (2010) Multi-beam X-ray source breast tomosynthesis reconstruction with different algorithms. Proc SPIE 7622H:1–8

14. Dobbins JT III, Godfrey DJ (2003) Digital X-ray tomosynthesis: current state of the art and clinical potential. Phys Med Biol 48:65–106
15. Zhao B, Zhao W (2008) Three-dimensional linear system analysis for breast tomosynthesis. Med Phys 35:5219. doi:10.1118/1.2996014
16. Gonzalez RC, Woods RE (2002) Digital Image Processing. Second Edition, Prentice Hall
17. Smith L: A Tutorial on Principal Components Analysis, www.cs.otago.ac.nz/cosc453/student_tutorials/principal_components.pdf, 2002.
18. Yang G, Rajaram R, Cao G, Sultana S, Liu Z, Lalush D, Lu JP, Zhou O (2008) Stationary digital breast tomosynthesis system with a multi-beam field emission x-ray source array. Proc SPIE 6913:69131A
19. CIRS Company. Stereotactic needle biopsy training phantom Model 013. Available at: http://www.cirsinc.com/products/all/44/stereotactic-needle-biopsy-training-phantom/. Accessed on August 9th, 2014.
20. Guimarães LTG, Schiabel H, Stemberg DRM (2009) Computer Simulation in Evaluating the Attenuation Coefficients Influence on Mammography Images Contrast. IFMBE Proc 25(2):454–457
21. Chen Y, Zhou W, Dobbins JT (2014) Fourier-Domain Methods for Optimization of Tomosynthesis (NEQ). book chapter in Tomosynthesis Imaging, ed. Reiser I and Glick S: Taylor & Francis